ACS PHYSICAL CHEMISTRY Au
AN OPEN ACCESS JOURNAL OF THE AMERICAN CHEMICAL SOCIETY

pubs.acs.org/physchemau

Article

A Bipolar CdS/Pd Photocatalytic Membrane for Selective Segregation of Reduction and Oxidation Processes

Federica Costantino, Luca Gavioli, and Prashant V. Kamat*

Cite This: *ACS Phys. Chem Au* 2022, 2, 89–97

Read Online

ACCESS | Metrics & More | Article Recommendations | Supporting Information

ABSTRACT: A photocatalytically active bipolar membrane consisting of a CdS photocatalyst and Pd electrocatalyst has been constructed to carry out environmentally relevant oxidation and reduction processes. The ion exchange property of a bipolar membrane (BPM) has allowed us to load the CdS photocatalyst on one side and Pd electrocatalyst on the other side. By inserting the photocatalytic BPM-CdS/Pd membrane between the two compartments of an H-cell, we can separate the reduction and oxidation processes. Following visible light excitation of CdS in the BPM-CdS/Pd membrane, we can induce vectorial electron transfer from CdS to Pd and to an electron acceptor (4-nitrophenol). The holes generated at CdS are scavenged by ethanol or 4-chlorophenol. The photocatalytic reduction rate dependence on the Pd loading in the membrane as well as its effect on modulating the rates of electron and hole transfer processes are discussed. The design of a semiconductor and metal loaded membrane paves the way for improving selectivity and efficiency of photocatalytic processes.

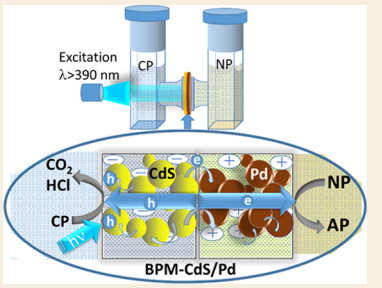

KEYWORDS: *photocatalysis, bipolar membrane, electron transfer, CdS, palladium, environmental remediation*

INTRODUCTION

Bipolar membranes, which have the capability of selective exchange of cations and anions, have been the topic of many recent investigations in electrocatalysis and photocatalysis.[1−10] In the majority of these examples, the membrane separates the anode and cathode compartments and thus allows for effective separation of products. Photocatalyst-loaded bipolar membranes have facilitated unassisted water splitting under photoirradiation.[3,4,11−13] The membrane-based assemblies that support gas diffusion electrodes in particular are at the heart of hydrogen fuel cells.[14,15] The same strategy of designing a membrane assembly with supported electrocatalysts in gas diffusion electrodes has been employed in a CO_2 reduction reaction.[1,2,8] Typically, a cation exchange membrane (e.g., Nafion) is employed to selectively transport protons across two compartments. A single-pass CO_2 conversion Faradaic efficiency of 85% for C_2 products using a modified cation exchange membrane has been reported recently.[16]

Cation- or anion exchange membranes transport cations or anions selectively when used as a separator between two electrochemical (or photocatalytic) compartments. Membranes such as Nafion have a high degree of SO_3^- moieties, which selectively bind cations, while repelling anions. On the other hand, bipolar membranes consist of two fused polymeric films capable of exchanging cations and anions separately. This unique feature allows the bipolar membrane to dissociate water molecules within the assembly as H^+ and OH^- ions with a pH difference as high as 10.[3,17] This property in turn allows an internal membrane potential of ∼600 mV to drive a photocatalytic or electrocatalytic reaction near the membrane surface. Bipolar membranes have been successfully employed to support electrocatalysts in the water splitting reaction.[4,5] Recent efforts have focused on the development of gas diffusion electrodes separated by BPM, for conducting CO_2 reduction with a continuous flow.[8,16,18]

Another interesting feature of an ion-exchangeable membrane is its ability to exchange with metal cations or anionic complexes. For example, Cd^{2+} ions can be easily embedded into Nafion by simply immersing in an aqueous solution. If this Cd^{2+}-loaded Nafion film is exposed to a sulfur (or selenium) source, one can readily make CdS (or CdSe) nanoparticles.[19−21] The void spaces (of 10−100 nm) within the Nafion film allow the size control of CdS nanoparticles in the quantized domain. Such semiconductor-loaded Nafion films have been extensively studied to explore their photocatalytic properties.[22−24] Although the demonstration of integrated chemical systems with CdS-loaded Nafion was elegantly demonstrated in photocatalysis in the 1980s,[22] the use of such photocatalytically active membranes in other photocatalytic applications remains rather limited.[25] In a recent study, we have demonstrated that semiconductor (CdS) and metal (Au) nanoparticles can be selectively loaded in a bipolar

Received: September 30, 2021
Revised: October 27, 2021
Accepted: November 1, 2021
Published: November 11, 2021

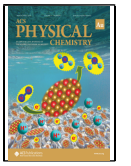

https://doi.org/10.1021/acsphyschemau.1c00035
ACS Phys. Chem Au 2022, 2, 89–97

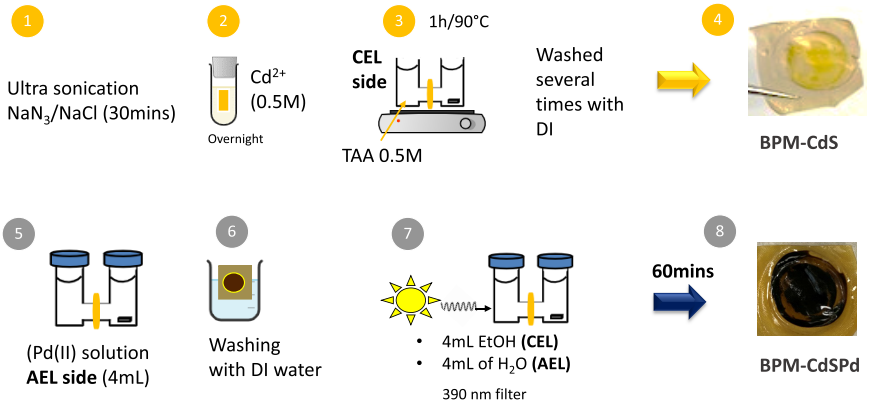

Figure 1. Synthetic steps involved in preparing a photocatalytic bipolar membrane. The schematic diagram illustrates key steps of loading the CdS photocatalyst in the CEL side (Steps 1−4) and Pd electrocatalysts on the AEL side (Steps 5−8) of the bipolar membrane.

membrane to create a photocatalytically active membrane.[10] The vectorial electron transfer across the photocatalytic membrane was confirmed from the excitation of CdS in the cation exchange layer (CEL) compartment and reduction of a methyl viologen radical in the anion exchange layer (AEL) compartment. Such a photocatalytic membrane can further aid in the remediation of organic pollutants.[26,27] We have now designed a CdS-Pd-based bipolar membrane to carry out selective reduction and oxidation processes. The design and properties of this photocatalytic membrane are discussed here.

EXPERIMENTAL SECTION

Chemicals and Materials

Sodium chloride (NaCl, >99%), sodium azide (NaN_3, >99%), methyl viologen dichloride (MV^{2+}, 98%), 4-nitrophenol (4-NP, 99%), and 4-chlorophenol (4-CP, 99%) were purchased from Sigma-Aldrich and used without purification. Ethanol (CH_3CH_2OH, 99%) was purchased from Kopatec. Thioacetamide (C_2H_5NS; TAA, 99.4%), cadmium nitrate tetrahydrate ($Cd(NO_3)_2{\cdot}4H_2O$, 99.99%), and tetraammine palladium chloride ($Pd(NH_3)_4Cl_2$, >99%) were purchased from Fisher Scientific. The bipolar membrane (BPM, PEEK supported) was purchased from Fuel Cell Store.

Characterization Methods

The absorption spectra were recorded using a Varian Cary 50 Bio UV−visible spectrometer. Pulse voltammetry was performed using a Gamry PCI 4750 in two-electrode cell setup, using Pt foil as a working electrode and Ag wire as a reference electrode. A 300 W Oriel xenon lamp was used as a light source along with a water filter (13 cm length) to remove infrared contributions. Long-pass filters were used for the different irradiation experiments to select the desired wavelength in the visible region. The cross-sectional SEM images were acquired with a Helios G4 Ux (FEI) at 5 kV. The samples were coated (Leica EM ACE600 sputter coater) with a 5 nm-thick carbon layer, to improve the electrical conductivity.

Fabrication of BPM-CdS

The bipolar membrane (initially soaked in 1 M NaCl and 100 ppm NaN_3 to exchange Na^+ ions) was cut in small pieces (2 cm × 2 cm^2). The film immersed in DI water was sonicated for 30 min and then copiously cleaned with DI water. The BPM was soaked in 0.5 M $Cd(NO_3)_2$ solution for 10 h to allow the adsorption of Cd^{2+} ions inside the pores of the cation exchange layer (CEL) side of the BPM. The membrane was rinsed with DI water and placed between the two compartments of the H-cell along with O-ring seals and clamps. The compartment facing the CEL side of the BPM was filled with 3 mL of TAA (0.5 M), while the AEL side was kept empty. The H-cell was placed in a preheated water bath at 90 °C for 1 h. At this temperature, TAA releases sulfur resulting in the formation of CdS, as reported in our previous study.[10]

Fabrication of BPM-CdS/Pd

The BPM/CdS membrane was thoroughly washed with water to remove any adsorbed ions in the surface. The BPM/CdS was inserted in the middle of the H-cell; the AEL side was exposed to 0.01 M solution of $Pd(NH_3)_4Cl_2{\cdot}H_2O$. The dissolved Pd(II) complex species can have various analogues including negatively charged species such as $[PdCl(NH_3)OH]^-$.[28] The adsorption time was varied starting from 5 to 120 min to achieve different loadings (see Table S1 in the Supporting Information for estimation of Pd(II) loading in the AEL layer). The BPM/CdS/Pd(II) film was washed with DI water to remove any adsorbed ions on the outside surface of the membrane and inserted in the H-cell. The CEL side of the compartment of the H-cell contained ethanol, while the AEL compartment contained water. Solutions were purged with N_2 for 30 min. The CEL side of the H-cell was irradiated for 60 min with a xenon lamp, using a cutoff filter (λ > 390 nm) in order to promote the growth of Pd in the AEL side of the membrane.

Photocatalytic Experiments Using BPM-CdS/Pd

The photocatalytic activity of the BPM-CdS/Pd membrane was monitored by measuring the change in solution absorbance upon irradiation of the H-cell. The BPM-CdS/Pd membrane was introduced between the arms of the cell. Solutions of probe molecules, such as methyl viologen (MV^{2+}), 4-nitrophenol (NP), and 4-chlorophenol (CP), were employed to establish the photoactivity of the membrane; the details can be found in the main text. Additional details of the photocatalytic setup and other tests are included in the Supporting Information.

The rate constant of the photodegradation process (k, min^{-1}) is calculated by fitting the experimental data with the pseudo-first-order kinetics model expressed in the equation $\ln \frac{A_0}{A} = kt$, where A_0 is the initial concentration of the probe species and A is the concentration of the solutions at time t during the photocatalytic process.

The degradation efficiency (%) is calculated using the following equation:

$$\text{degradation efficiency (\%)} = \frac{C_0 - C}{C_0} \times 100\%$$

RESULTS AND DISCUSSION

Designing a Photocatalytically Active Bipolar Membrane (BPM)

The ability to exchange cations and anions selectively in two parts of the bipolar membrane has allowed us to synthesize semiconductor and metal nanoparticles within the pores of the membrane. In the present study, we prepared a photocatalyti-

https://doi.org/10.1021/acsphyschemau.1c00035
ACS Phys. Chem Au 2022, 2, 89−97

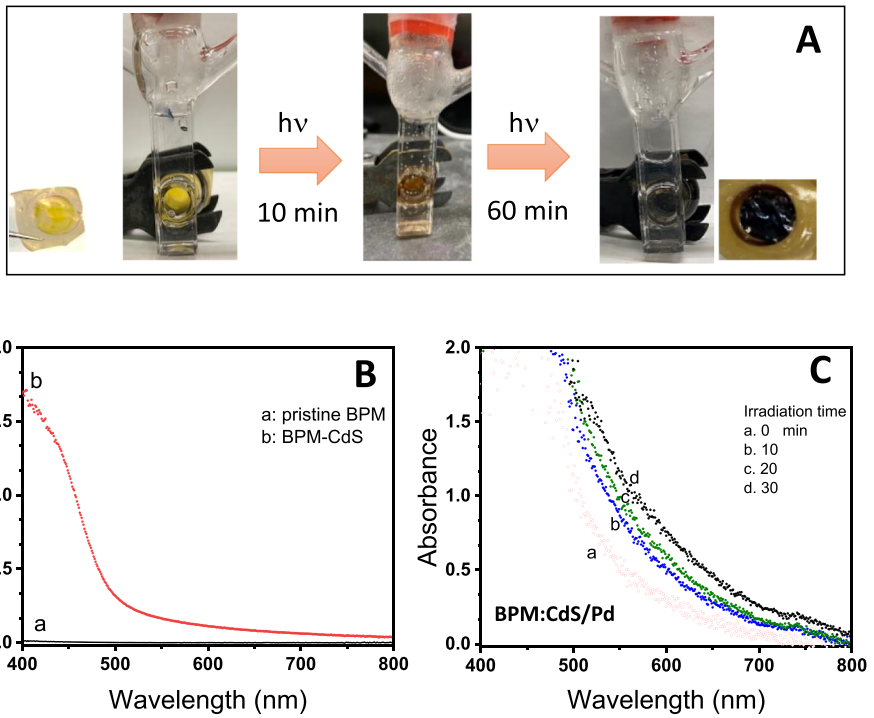

Figure 2. (A) Color change of the BPM associated with the formation of CdS in the CEL (left) followed by 10 and 60 min irradiations to produce Pd nanoparticles in the AEL (right). (B) Absorbance spectra of BPM-CdS following the exposure of the Cd^{2+}-loaded CEL layer to thioacetamide. (C) Absorbance spectra of BPM-CdS/Pd(II) recorded during the growth of Pd nanoparticles in the AEL side. The CdS in the BPM was excited with visible light to provide photogenerated electrons for Pd reduction (with holes scavenged by ethanol in the H-cell).

cally active BPM by exchanging Cd^{2+} in the cation exchange layer (CEL) and Pd(II) in the anion exchange layer (AEL). The schematic illustration of synthesis of CdS-Pd bipolar membrane is presented in Figure 1, based on our earlier demonstration of preparing aC dS-Au photocatalytic membrane.[10] The Cd^{2+}-loaded bipolar membrane was first transformed into CdS by reacting with thioacetamide (Steps 1−4 in Figure 1). To form Pd nanoparticles within the BPM, we then reduced Pd(II) in the AEL by exciting CdS (CEL) with visible light in a H-cell. The excitation of CdS generates electrons and holes within the film. As the holes are scavenged by ethanol, the electrons are transported to the AEL and reduce $(PdCl_4)^{2-}$ ions (Steps 5−8 in Figure 1). The overall processes leading to the formation of CdS and Pd in the two parts of the BPM are expressed in reactions 1 and 2.

Part 1

$$\text{CEL-Na}^+ + \text{Cd}^{2+} \rightarrow \text{CEL-Cd}^{2+} \quad (1a)$$

$$\text{CEL-Cd}^{2+} + \text{thioacetamide} \rightarrow \rightarrow \text{CEL-CdS} \quad (1b)$$

Part 2

$$\text{AEL-Cl}^- + \text{Pd(II)} \rightarrow \text{AEL-Pd(II)} \quad (2a)$$

$$\text{AEL-Pd(II)} + \text{CEL-CdS (e)} \rightarrow \rightarrow \text{AEL-Pd}^0 + \text{CEL-CdS} \quad (2b)$$

The formation of CdS in the CEL and Pd in the AEL can be visualized through color changes as shown in the photographs of the membrane following the two-part synthesis (Figure 2A). The changes in the absorption spectra are shown in Figure 2B,C. The CdS nanoparticles formed within the pores of the membrane exhibit an absorption onset around 490 nm (or 2.53 eV), which is close to the bandgap energy of the bulk semiconductor (E_g = 2.42 eV). Similarly, the formation of Pd in the AEL is marked by the broad absorption in the visible range. Because of the strong absorption and scattering effects, the absorption spectra of the Pd-loaded film could not be analyzed. It is interesting to note that these spectral features confirm the loading of the semiconductor and metal nanoparticles within the pores of the membrane.

Figure 3 shows the cross-sectional SEM image of the BPM-CdS/Pd membrane at two different magnifications. The overall thickness of the membrane is ∼100 μm with two distinct layers loaded with CdS and Pd nanoparticles. The particle morphologies of these two layers enable distinction between the CEL and AEL of the BPM. The elemental analyses of these

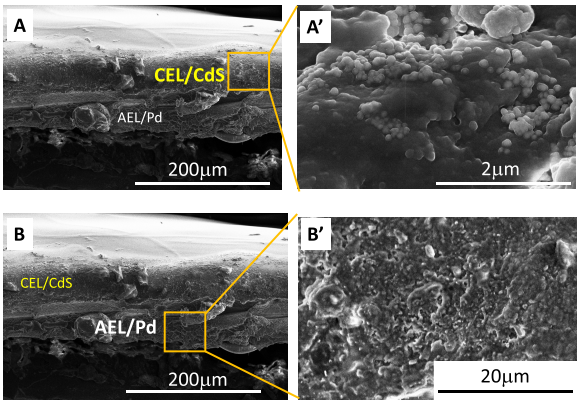

Figure 3. Cross-sectional image of the BPM-CdS/Pd membrane. (A, A′) CEL at two different magnifications showing the CdS particles and (B, B′) AEL loaded with Pd particles at two different magnifications. Additional images and elemental analysis are included in the Supporting Information, Figures S1 and S2.

https://doi.org/10.1021/acsphyschemau.1c00035
ACS Phys. Chem Au 2022, 2, 89−97

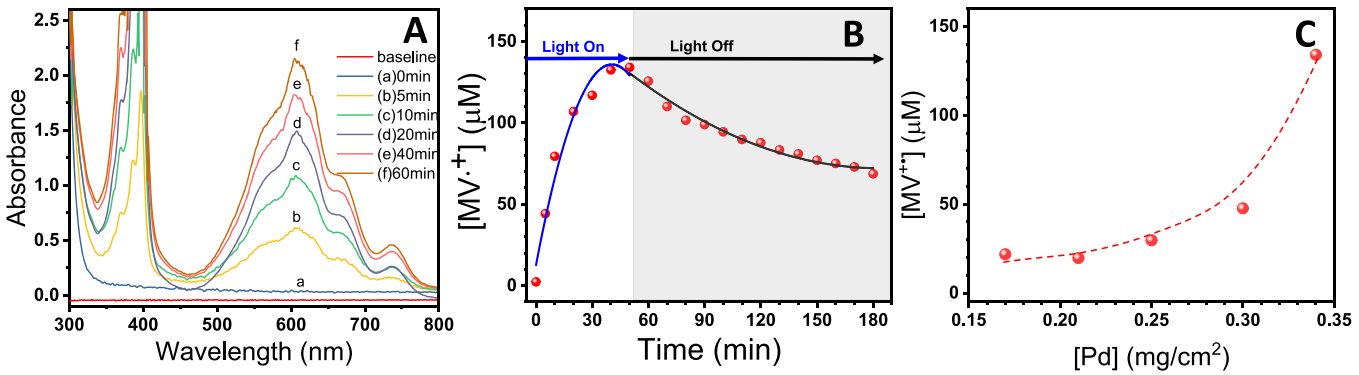

Figure 4. (A) Formation of $MV^{+\bullet}$ as monitored from the absorption spectra recorded during the excitation of BPM-CdS/Pd with visible light. Deaerated ethanol solution MV^{2+} (1 mM) was employed in the AEL compartment. Pd loading in the BPM was 0.34 mg/cm^2. (B) Formation of $MV^{+\bullet}$ under visible light irradiation ($\lambda > 390$ nm) and its decay upon stopping the illumination. (C) Dependence of the steady-state concentration of $MV^{+\bullet}$ on the loading of Pd in the BPM-CdS/Pd membrane.

particles and other cross-sectional image of the blank film are included in the Supporting Information (see Figures S1 and S2). From Figure 3A′, we estimate that the CEL consists of 70−100 nm diameter CdS nanoparticles (the size distribution analysis is reported in Figure S3). The Pd particles loaded in the AEL on the other hand exhibit both particle- and rod-like structures (Figure 3B′). These images provide a glimpse of photocatalysts and Pd nanoparticles embedded in two separate layers of the bipolar membrane. The elemental analysis images show a relatively small fraction of Pd and CdS nanoparticles in the opposing sides (viz., CEL and AEL sides, respectively). Such crossover effect, if any, should be beneficial in maintaining the continuity for shuttling electrons between excited CdS and Pd nanoparticles.

Optimization of Pd Loading in the AEL

In order to optimize the photocatalytic membrane, we wanted to vary the concentration of photocatalysts and metal catalysts. For CdS loading, the NaN_3/NaCl-treated membrane was soaked in Cd^{2+} solution overnight. This procedure allowed us to maximize the concentration of CdS in the photocatalytic BPM so that we can capture incident photons. We varied the concentration of Pd(II) in the AEL before subjecting it to photocatalytic reduction. The concentration was varied by soaking the CdS-loaded BPM in $Pd(NH_3)_4Cl_2$ solution for several different times. We monitored the loss of Pd(II) in solution to estimate the amount that incorporated in the AEL. The Pd(II) concentration in solution was monitored using the absorption spectra and square wave voltammetry. Details of Pd(II) loading in the AEL are given in the Supporting Information (Figures S4 and S5).

We loaded five separate BPMs with a constant amount of CdS but varying amounts of Pd loading and tested the photocatalytic activity of each membrane. We probed the photocatalytic activity through the reduction of methyl viologen in the AEL compartment of the H-cell. The BPM-CdS/Pd membrane was inserted in the middle of the H-cell, separating the solutions in the CEL and AEL compartments. The arms of the cell were made from quartz cuvette, allowing us to probe the changes in the absorption of the respective solution in each compartment. Photoexcitation was conducted through the CEL side so that CdS can be excited to induce the photocatalytic reaction. The area of the film exposed to light was 0.785 cm^2. As ethanol in the CEL compartment scavenged the photogenerated holes, the electrons accumulated in CdS get transferred to the Pd nanoparticles embedded in the AEL. Although these two layers are physically separated, the crossover of the particles at opposite sides provides continuity for electron shuttling across the entire membrane. MV^{2+} present in the AEL compartment captured these electrons to form the reduced methyl viologen cation radical ($MV^{+\bullet}$). Because of the positive charge for both MV^{2+} and $MV^{+\bullet}$, they remain in solution and are repelled by the AEL part of the membrane.

Reactions 3−6 represent the reduction of MV^{2+} following the photoexcitation of CdS in the BPM-CdS/Pd membrane.

$$\text{BPM-CdS/Pd} + h\nu \rightarrow \text{BPM-CdS}(h - e)/\text{Pd} \quad (3)$$

$$\text{BPM-CdS}(h - e)/\text{Pd} + C_2H_5OH \rightarrow \text{BPM-CdS}(e)/\text{Pd} + C_2H_5O^{\bullet} \quad (4)$$

$$\text{BPM-CdS}(e)/\text{Pd} \rightarrow \text{BPM-CdS/Pd}(e) \quad (5)$$

$$\text{BPM-CdS/Pd}(e) + MV^{2+} \rightarrow \text{BPM-CdS/Pd} + MV^{+\bullet} \quad (6)$$

The formation of the reduction product $MV^{+\bullet}$ in the AEL compartment was monitored by recording the absorption spectra (Figure 4A). With continued irradiation of visible light, we see increased absorption in the visible range with characteristic $MV^{+\bullet}$ peaks at 395 and 610 nm, respectively.[29] From the $MV^{+\bullet}$ extinction coefficient at 610 nm (13,700 M^{-1} cm^{-1}),[29] we determined the concentration of $MV^{+\bullet}$ formed in the AEL compartment. With increasing photoirradiation time, the $MV^{+\bullet}$ attained a a steady-state concentration of 135 μM (Figure 4B). As indicated in our earlier study,[30] metal nanoparticles are also capable of accepting electrons to catalyze other reduction processes (reaction 7).

$$\text{BPM-CdS/Pd} + MV^{+\bullet} \rightarrow \text{BPM-CdS/Pd}(e) + MV^{2+} \quad (7)$$

For example, the electron transfer between photogenerated $MV^{+\bullet}$ and metal nanoparticles has been investigated for H_2 generation in aqueous solutions.[31−33] The interesting aspect of attaining the steady-state concentration of $MV^{+\bullet}$ during steady-state irradiation is the result of forward (reaction 6) and back (reaction 7) electron transfer. The plot in Figure 4B shows the growth of $MV^{+\bullet}$ during visible light irradiation attaining a steady state in ∼60 min. Upon fitting the growth of $MV^{+\bullet}$ concentration to pseudo-first-order kinetics, we obtain a rate

https://doi.org/10.1021/acsphyschemau.1c00035
ACS Phys. Chem Au 2022, 2, 89−97

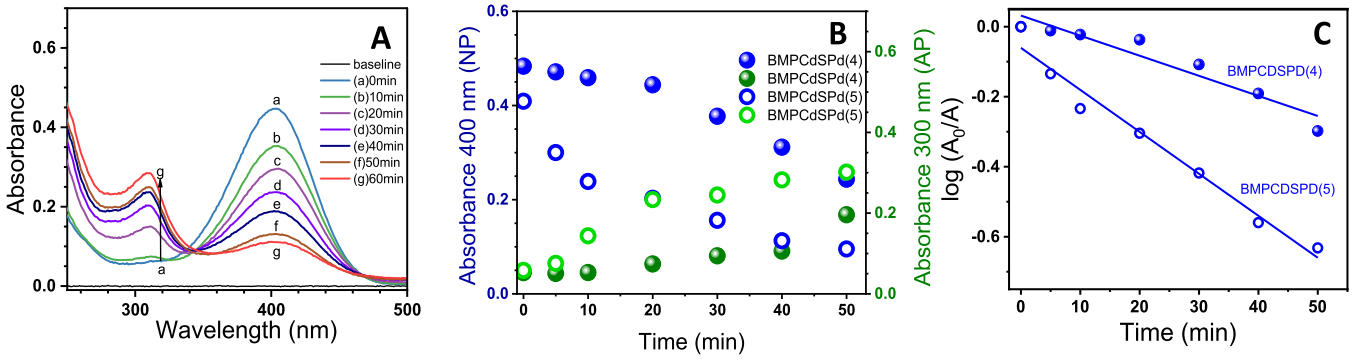

Figure 5. Photocatalytic reduction of 25 μM 4-nitrophenol in water (AEL compartment) during the visible light irradiation of BPM-CdS/Pd. (A) Absorption spectra of AEL compartment solution recorded at different irradiation times ([Pd] in the membrane = 0.34 mg/cm^2). (B) Decrease of 4-NP absorbance at 400 nm and growth of 4-AP absorbance at 300 nm at two different Pd Loadings (0.30 (solid circles) and 0.34 (open circles) mg/cm^2 Pd). (C) Pseudo-first-order kinetic analysis for the decay of 4-NP at two different Pd loadings (Pd(4) = 0.30 (solid circles) and Pd(5) = 0.34 (open circles) mg/cm^2 Pd). The CEL compartment contained 3:1 ethanol/water by volume for these experiments.

constant of 5×10^{-3} min^{-1}. Upon stopping the illumination, the back electron transfer results in a decrease in $MV^{+\bullet}$ concentration (Figure 4B). We estimate the rate constant for back electron transfer to be 2×10^{-3} min^{-1}. The difference between forward and back electron transfer dictates the steady-state concentration.

The estimate of steady-state concentration of $MV^{+\bullet}$ also allows us to estimate the flat band potential of the BPM-CdS/Pd membrane using the Nernst expression (expression 8).[34]

$$E_{FB} = E^0(MV^{2+}/MV^{+\bullet}) - 0.059 \log[MV^{+\bullet}]/[MV^{2+}] \quad (8)$$

By substituting the steady-state concentrations of $MV^{+\bullet}$ and MV^{2+} along with the redox potential of the $MV^{2+}/MV^{+\bullet}$ couple, $E^\circ = -0.449$ V vs NHE,[35] we obtain E_{FB} as -0.460 V vs NHE. This estimation of E_{FB} provides the energetics of the membrane with which it can induce redox processes.

We repeated the above experiment with four other BPM-CdS/Pd membranes having different loadings of Pd (0.17–0.30 mg/cm^2), see Figures S6 and S7 in the Supporting Information. The steady-state concentrations achieved with these membranes are presented in Figure 4C. It is evident that the increased Pd loading leads to the increased $MV^{+\bullet}$ concentration, indicating that the high loading of Pd is required to capture the photogenerated electrons from CdS and transfer to MV^{2+} in the AEL compartment. These experiments confirm the vectorial electron transfer from the CEL compartment to the AEL compartment induced through the excitation of the BPM-CdS /Pd membrane.

Reduction of 4-Nitrophenol

Semiconductor-assisted photocatalysis has been widely studied in the remediation of organic pollutants from air and water.[36−38] Of particular interest are nitroaromatic compounds such as nitrophenol and trinitrophenol that are environmental water contaminants.[39,40] In order to test the feasibility of the BPM-CdS/Pd membrane for degradation of nitroaromatics, we employed 4-nitrophenol (NP) as a representative in the AEL compartment. The experiments were done in a similar fashion as in the case of MV^{2+}reduction. We introduced an aqueous solution of NP with pH adjusted to 10 so that it exists in solution as nitrophenoxide ion ($pK_a \approx 7$)[41] with an absorption maximum at 400 nm. Since the absorbance of NP remains unchanged in solution after extended contact with the BPM-CdS/Pd in the dark, we rule out any incorporation of NP in the AEL.

The H-cell containing BPM-CdS/Pd with ethanol (hole scavenger) in the CEL compartment and 25 μM NP in the AEL compartment was subjected to visible light excitation ($\lambda >$ 390 nm). The absorption spectrum of the solution in the AEL compartment was recorded periodically during photoirradiation of the CdS side of the BPM-CdS/Pd membrane. The vectorial flow of electrons from CdS to Pd resulted in the reduction of NP to 4-amino phenol (AP). The decrease in NP absorption at 400 nm coincided with the increase in the absorption of AP at 310 nm, as can be noted from Figure 5A. The decrease in absorption at 400 nm and growth of absorption at 300 nm with irradiation time are shown in Figure 5B for two different Pd concentrations. The kinetic analysis of 4-NP decay (Figure 5C) shows a pseudo-first-order degradation rate of 6×10^{-3} and 1×10^{-2} s^{-1} for Pd catalyst loadings of 0.30 and 0.34 mg/cm^2, respectively, in the BPM-CdS/Pd membrane. This increase in rate constant with increased metal nanoparticle loading follows the trend seen with MV^{2+} reduction seen in Figure 4C. The results further establish the effectiveness of the BPM-CdS/Pd membrane in the photocatalytic reduction of 4-NP.

A BPM-CdS/Pd Membrane for Simultaneous Reduction and Oxidation of Pollutants

Organochlorines have been widely used as pesticides and wood treatment chemicals.[38,42,43] Their contamination of soil, water, and food products are of concern.[43−46] Advanced oxidation processes such as photocatalysis are quite effective in the remediation of such organochlorines.[38] In order to utilize the photocatalytic oxidation, we employed a model pollutant, 4-chlorophenol (CP), in the CEL compartment along with NP solution in the AEL compartment. CP has been used as a model pollutant to investigate the photocatalytic mineralization of organochlorines.[47−49] By replacing ethanol with CP as the electron donor in the CEL compartment, we can maintain the stability of CdS during photoirradiation. This configuration allowed us to degrade two model pollutants simultaneously using the BPM-CdS/Pd membrane.

The H-cell containing aqueous solutions of 30 μM CP in the CEL compartment and 30 μM NP in the AEL compartment separated by the BPM-CdS/Pd membrane was irradiated with visible light ($\lambda >$ 390 nm). As the CdS in the membrane absorbed light to generate electrons and holes, we observed a

https://doi.org/10.1021/acsphyschemau.1c00035
ACS Phys. Chem Au 2022, 2, 89−97

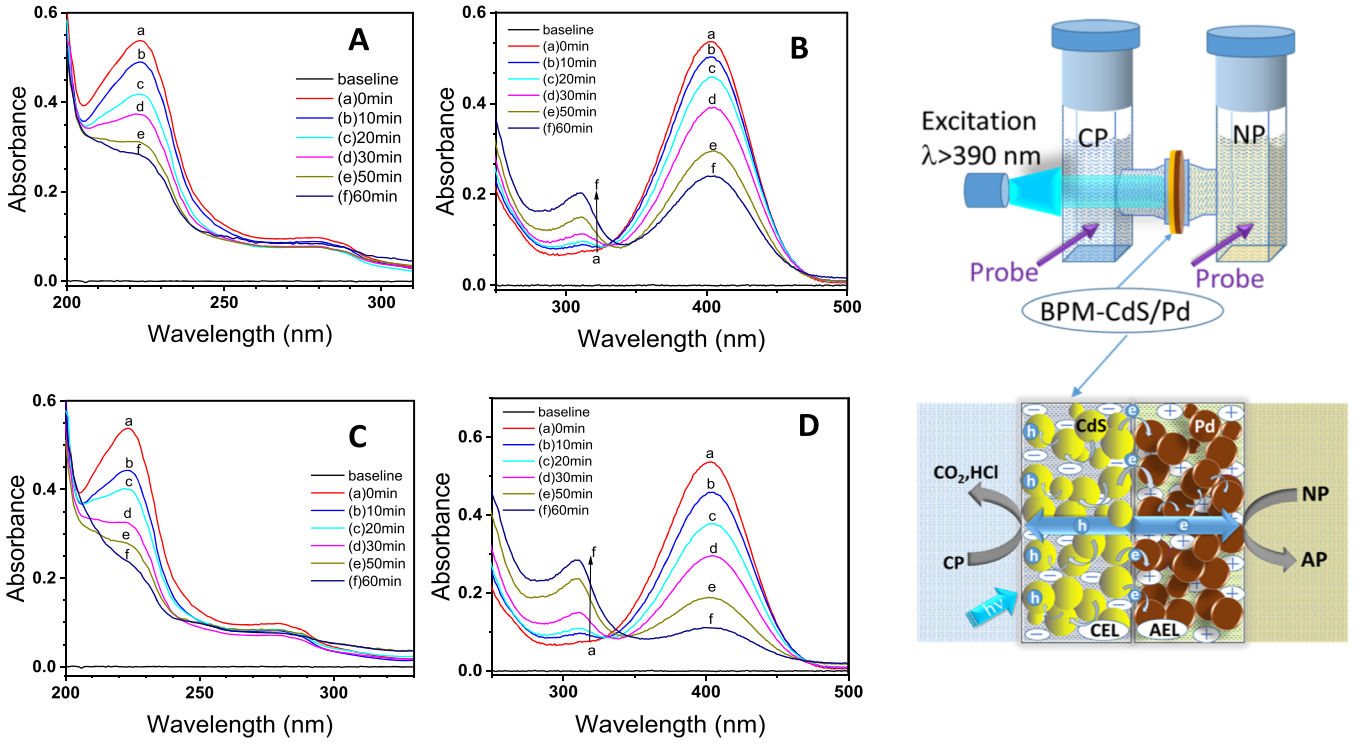

Figure 6. Absorption changes of (A, C) 4-chlorophenol (30 μM aqueous solution in the CEL compartment) and (B, D) 4-nitrophenol (30 μM aqueous solution in the AEL compartment) recorded during the visible light (>390 nm) irradiation of BPM-CdS/Pd at two different Pd loadings: (A, B) 0.30 mg/cm^2 and (C, D) 0.34 mg/cm^2 Pd. The scheme on the right illustrates the cell configuration and mechanism of degradation of two model compounds.

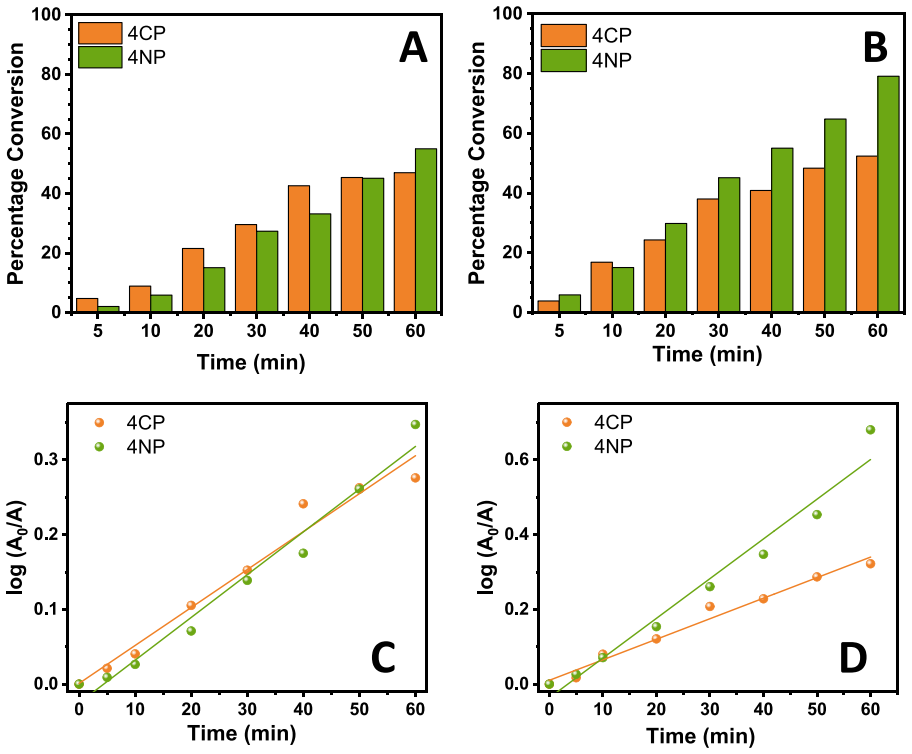

Figure 7. Percentage conversion of 4-chlorophenol (CP; 30 μM in the CEL compartment) and 4-nitrophenol (NP; 30 μM in the AEL compartment) monitored during the visible light (λ > 390 nm) irradiation of BPM-CdS/Pd at two different Pd loadings: (A) 0.30 and (B) 0.34 mg/cm^2 Pd. (C, D) Corresponding first-order plots.

decreasing absorption of the parent compound in the two compartments. Figure 6 shows the changes in the absorption of NP and CP at different irradiation times. These changes in the absorption can be related to the oxidation of CP by the

https://doi.org/10.1021/acsphyschemau.1c00035
ACS Phys. Chem Au 2022, 2, 89−97

holes generated at CdS and reduction of NP at the Pd interface (reactions 9−11).

Membrane:

$$\text{BPM-CdS/Pd} + h\nu \rightarrow \text{BPM-CdS(h} - \text{e)/Pd} \rightarrow \text{BPM-CdS(h)/Pd(e)} \quad (9)$$

CEL compartment:

$$\text{BPM-CdS(h)/Pd} + \text{CP} \rightarrow \text{BPM-CdS/Pd} + (\text{chlorocatechol, hydroquinone, ...}) \rightarrow \rightarrow CO_2 + \text{HCl} \quad (10)$$

AEL compartment:

$$\text{BPM-CdS/Pd(e)} + \text{NP} \rightarrow \text{BPM-CdS/Pd} + \text{AP} \quad (11)$$

Figure 6A,C shows the changes in the absorption spectra of CP as we subject the BPM-CdS/Pd membranes (with different Pd loadings) to photoirradiation. The decrease in absorbance at 300 nm is indicative of degradation of CP as it reacts with the holes generated at CdS. As shown earlier, the photocatalytic oxidation of CP results in the formation of chlorocatechol and hydroquinone as major intermediates with ultimate conversion to CO_2 and HCl (reaction 10).[49] The detailed mechanism of photocatalytic oxidation can be found in our earlier studies.[49−51] The absorption changes of the solution in the AEL compartment (Figure 6B,D) confirm the transformation of NP to AP (reaction 11). In the present experiments, we monitored the degradation of 4-CP and compared it with NP degradation in the AEL compartment.

Figure 7A,B compares the percent conversion of CP and NP with irradiation time at two different Pd loadings of 0.30 and 0.34 mg/cm^2. At a lower Pd concentration, the percent degradations of NP and CP are similar, and we achieve about 50% degradation during 60 min light irradiation. On the other hand, with higher Pd loading, we see a higher degree of NP degradation, while the CP degradation remains almost the same. We also analyzed the decay of CP and NP using pseudo-first-order kinetic analysis (Figure 7C,D). The rate constants for degradation are presented in Table 1.

Table 1. Rate Constant Analysis for the Photocatalytic Degradation of CP and NP Using BPM-CdS/Pd

Pd loadings (mg/cm^2)	CP k (min^{-1})	NP k (min^{-1})
0.30	0.005 (R^2 = 0.96)	0.005 (R^2 = 0.97)
0.34	0.006 (R^2 = 0.96)	0.01 (R^2 = 0.97)

It is interesting to note that at a lower Pd concentration, the rate constants of the two degradations are closely matched. The similarity of the two rate constants explains achieving constant conversion between the two model contaminants (*viz.*, CP and NP) at lower Pd loading in the membrane. The higher rate constant of degradation at 0.34 mg/cm^2 Pd loadings explains the higher percent of degradation of NP. Since we maintain similar loading of CdS, we see a similar rate of degradation as well as similar fraction of degradation of CP in AEL compartments. These results show that one can modulate the degradation rates of organic contaminants in AEL and CEL compartments by controlling the loading of the photocatalyst and metal nanoparticles in the BPM. In order to maintain the stability of the photocatalyst and electrocatalyst in the BPM membrane and maximize the photoconversion efficiency, one needs to balance the rates of both reduction and oxidation processes.

CONCLUSIONS

A bipolar membrane with specific cation exchange and anion exchange properties between the two layers enables design of a photocatalytically active membrane that also separates reaction compartments. The key advantage of such a membrane lies in the separation of oxidation and reduction processes while continuing to engage in the photodriven reactions. The example of simultaneous oxidation of 4-chlorophenol and the reduction of 4-nitrophenol under visible light irradiation of the BPM-CdS/Pd shows its effectiveness in photocatalytic remediation of chemical contaminants. Efforts are underway to extend the design of the photocatalytic membrane in a flow cell design. By controlling the flow rates and the intensity of excitation, it should be possible to implement the photocatalytic membrane in a continuous flow reactor.

ASSOCIATED CONTENT

Supporting Information

The Supporting Information is available free of charge at https://pubs.acs.org/doi/10.1021/acsphyschemau.1c00035.

Additional supporting results related to SEM analysis, determination of Pd loadings, and the Pd loading effect on MV^{2+} reduction are included (PDF)

AUTHOR INFORMATION

Corresponding Author

Prashant V. Kamat − *Notre Dame Radiation Laboratory, University of Notre Dame, Notre Dame, Indiana 46556, United States; Department of Chemistry and Biochemistry, University of Notre Dame, Notre Dame, Indiana 46556, United States;* orcid.org/0000-0002-2465-6819; Email: pkamat@nd.edu

Authors

Federica Costantino − *Notre Dame Radiation Laboratory, University of Notre Dame, Notre Dame, Indiana 46556, United States; Department of Chemistry and Biochemistry, University of Notre Dame, Notre Dame, Indiana 46556, United States; Intersciplinary Laboratories for Advanced Materials Physics (I-LAMP) and Dipartimento di Matematica e Fisica, Università Cattolica del Sacro Cuore, Brescia 25133, Italy; Smart Materials, Istituto Italiano di Tecnologia (IIT), 16163 Genova, Italy*

Luca Gavioli − *Intersciplinary Laboratories for Advanced Materials Physics (I-LAMP) and Dipartimento di Matematica e Fisica, Università Cattolica del Sacro Cuore, Brescia 25133, Italy;* orcid.org/0000-0003-2782-7414

Complete contact information is available at: https://pubs.acs.org/10.1021/acsphyschemau.1c00035

Notes

The authors declare no competing financial interest.

ACKNOWLEDGMENTS

P.V.K. acknowledges support by the Division of Chemical Sciences, Geosciences, and Biosciences, Office of Basic Energy

Sciences of the U.S. Department of Energy (award DE-FC02-04ER15533), and F.C. acknowledges the support of the Catholic University of Sacred Heart (UCSC, Italy) and Italian Institute of Technology (IIT, Italy) to conduct research at the University of Notre Dame. The authors also kindly acknowledge Dr. Despina Fragouli for discussions and Bo-An Chen for the acquisition of the HR-SEM images. This is NDRL 5337 from the Notre Dame Radiation Laboratory.

REFERENCES

(1) Weekes, D. M.; Salvatore, D. A.; Reyes, A.; Huang, A. X.; Berlinguette, C. P. Electrolytic CO_2 Reduction in a Flow Cell. *Acc. Chem. Res.* **2018**, *51*, 910−918.
(2) Salvatore, D. A.; Weekes, D. M.; He, J.; Dettelbach, K. E.; Li, Y. C.; Mallouk, T. E.; Berlinguette, C. P. Electrolysis of Gaseous CO_2 to CO in a Flow Cell with a Bipolar Membrane. *ACS Energy Lett.* **2018**, *3*, 149−154.
(3) Vermaas, D. A.; Sassenburg, M.; Smith, W. A. Photo-assisted Water Splitting with Bipolar Membrane Induced pH Gradients for Practical Solar Fuel Devices. *J. Mater. Chem. A* **2015**, *3*, 19556−19562.
(4) Chabi, S.; Wright, A. G.; Holdcroft, S.; Freund, M. S. Transparent Bipolar Membrane for Water Splitting Applications. *ACS Appl. Mater. Interfaces* **2017**, *9*, 26749−26755.
(5) Sun, K.; Liu, R.; Chen, Y.; Verlage, E.; Lewis, N. S.; Xiang, C. A Stabilized, Intrinsically Safe, 10% Efficient, Solar-Driven Water-Splitting Cell Incorporating Earth-Abundant Electrocatalysts with Steady-State pH Gradients and Product Separation Enabled by a Bipolar Membrane. *Adv. Energy Mater.* **2016**, *6*, 1600379.
(6) Manohar, M.; Kim, D. Advantageous of Hybrid Fuel Cell Operation under Self-Humidification for Energy Efficient Bipolar Membrane. *ACS Sustainable Chem. Eng.* **2019**, *7*, 16493−16500.
(7) Eisaman, M. D.; Alvarado, L.; Larner, D.; Wang, P.; Garg, B.; Littau, K. A. CO_2 Separation using Bipolar Membrane Electrodialysis. *Energy Environ. Sci.* **2011**, *4*, 1319−1328.
(8) Li, Y. C.; Zhou, D.; Yan, Z.; Gonçalves, R. H.; Salvatore, D. A.; Berlinguette, C. P.; Mallouk, T. E. Electrolysis of CO_2 to Syngas in Bipolar Membrane-Based Electrochemical Cells. *ACS Energy Lett.* **2016**, *1*, 1149−1153.
(9) Chou, T.-J.; Tanioka, A. Current−Voltage Curves of Composite Bipolar Membrane in Alcohol−Water Solutions. *J. Phys. Chem. B* **1998**, *102*, 7866−7870.
(10) Chhetri, M.; Kamat, P. V. Vectorial Charge Transfer across Bipolar Membrane Loaded with CdS and Au Nanoparticles. *J. Phys. Chem. C* **2021**, *125*, 6870−6876.
(11) Smotkin, E.; Bard, A. J.; Campion, A.; Fox, M. A.; Mallouk, T.; Webber, S. E.; White, J. M. Bipolar TiO_2/Pt Semiconductor Photoelectrodes and Multielectrode Arrays for Unassisted Photolytic Water Splitting. *J. Phys. Chem.* **1986**, *90*, 4604−4607.
(12) Park, J. H.; Bard, A. J. Unassisted Water Splitting from Bipolar Pt/Dye-Sensitized TiO_2 Photoelectrode Arrays. *Electrochem. Solid-State Lett.* **2005**, *8*, G371−G375.
(13) Mayerhöfer, B.; McLaughlin, D.; Böhm, T.; Hegelheimer, M.; Seeberger, D.; Thiele, S. Bipolar Membrane Electrode Assemblies for Water Electrolysis. *ACS Appl. Energy Mater.* **2020**, *3*, 9635−9644.
(14) Tollefson, J. Car industry: Fuel of the Future? Hydrogen fuel-cell vehicles, largely forgotten as attention turned to biofuels and batteries, are staging a comeback. *Nature* **2010**, *464*, 1262−1264.
(15) Wagner, F.; Lakshmanan, B.; Mathias, M. Electrochemistry and the Future of the Automobile. *J. Phys. Chem. Lett.* **2010**, *1*, 2204−2219.
(16) O'Brien, C. P.; et al. Single Pass CO_2 Conversion Exceeding 85% in the Electrosynthesis of Multicarbon Products via Local CO_2 Regeneration. *ACS Energy Lett.* **2021**, *6*, 2952−2959.
(17) Oener, S. Z.; Foster, M. J.; Boettcher, S. W. Accelerating Water Dissociation in Bipolar Membranes and for Electrocatalysis. *Science* **2020**, 1099−1103.
(18) Cheng, W.-H.; Richter, M. H.; Sullivan, I.; Larson, D. M.; Xiang, C.; Brunschwig, B. S.; Atwater, H. A. CO_2 Reduction to CO with 19% Efficiency in a Solar-Driven Gas Diffusion Electrode Flow Cell under Outdoor Solar Illumination. *ACS Energy Lett.* **2020**, *5*, 470−476.
(19) Mau, A. W. H.; Huang, C. B.; Kakuta, N.; Bard, A. J.; Campion, A.; Fox, M. A.; White, J. M.; Webber, S. E. H_2 Photoproduction by Nafion/CdS/Pt films in H_2O/S^{2-} Solutions. *J. Am. Chem. Soc.* **1984**, *106*, 6537−6542.
(20) Gopidas, K. R.; Kamat, P. V. Photoinduced charge transfer processes in ultrasmall semiconductor clusters. Photophysical properties of CdS clusters in Nafion membrane. *J. Chem. Sci.* **1993**, *105*, 505−512.
(21) Smotkin, E. S.; et al. Ultrasmall Particles of Cadmium Selenide and Cadmium Sulfide formed In nafion by an Ion-Dilution Technique. *J. Phys. Chem.* **1990**, *94*, 7543−7549.
(22) Krishnan, M.; White, J. R.; Fox, M. A.; Bard, A. J. Integrated Chemical Systems: Photocatalysis at Semiconductors Incorporated into Polymer (Nafion)/Mediator Systems. *J. Am. Chem. Soc.* **1983**, *105*, 7002−7003.
(23) Hara, M.; Mallouk, T. E. Photocatalytic water oxidation by Nafion-stabilized iridium oxide colloids. *Chem. Commun.* **2000**, 1903−1904.
(24) Park, H.; Park, Y.; Bae, E.; Choi, W. Photoactive Component-loaded Nafion Film as a Platform of Hydrogen Generation: Alternative Utilization of a Classical Sensitizing System. *J. Photochem. Photobiol., A* **2009**, *203*, 112−118.
(25) Zhang, H.; Wan, Y.; Luo, J.; Darling, S. B. Drawing on Membrane Photocatalysis for Fouling Mitigation. *ACS Appl. Mater. Interfaces* **2021**, *13*, 14844−14865.
(26) Wang, S.; Liu, P.; Wang, X.; Fu, X. Homogeneously Distributed CdS Nanoparticles in Nafion Membranes: Preparation, Characterization, and Photocatalytic Properties. *Langmuir* **2005**, *21*, 11969−11973.
(27) Vohra, M. S.; Tanaka, K. Enhanced Photocatalytic Activity of Nafion-Coated TiO_2. *Environ. Sci. Technol.* **2001**, *35*, 411−415.
(28) Zeizinger, M.; Burda, J. V.; Šponer, J.; Kapsa, V.; Leszczynski, J. A Systematic ab Initio Study of the Hydration of Selected Palladium Square-Planar Complexes. A Comparison with Platinum Analogues. *J. Phys. Chem. A* **2001**, *105*, 8086−8092.
(29) Watanabe, T.; Honda, K. Measurement of the Extinction Coefficient of the Methyl Viologen Cation Radical and The Efficiency of Its Formation by Semiconductor Photocatalysis. *J. Phys. Chem.* **1982**, *86*, 2617−2619.
(30) Harris, C.; Kamat, P. V. Photocatalytic Events of CdSe Quantum Dots in Confined Media. Electrodic Behavior of Coupled Platinum Nanoparticles. *ACS Nano* **2010**, *4*, 7321−7330.
(31) Nakahira, T.; Graetzel, M. Fast Electron Storage with Colloidal Semiconductors Functionalized with Polymeric Viologen. *J. Phys. Chem.* **1984**, *88*, 4006−4010.
(32) Graetzel, M.; Moser, J. Multielectron Storage and Hydrogen Generation with Colloidal Semiconductors. *Proc. Natl. Acad. Sci. U. S. A.* **1983**, *80*, 3129−3132.
(33) Meisel, D.; Mulac, W. A.; Matheson, M. S. Catalysis of Methyl Viologen Radical Reactions by Polymer- Stabilized Gold Sols. *J. Phys. Chem.* **1981**, *85*, 179−187.
(34) Fitzmaurice, D. Using Spectroscopy to Probe The Band Energetics of Transparent Nanocrystalline Semiconductor Films. *Sol. Energy Mater. Sol. Cells* **1993**, *32*, 289−305.
(35) Bird, C. L.; Kuhn, A. T. Electrochemistry of the Viologens. *Chem. Soc. Rev.* **1981**, *10*, 49−82.
(36) Ollis, D. F.; Pelizzetti, E.; Serpone, N. Photocatalyzed destruction of water contaminants. *Environ. Sci. Technol.* **1991**, *25*, 1522−1529.
(37) Hoffmann, M. R.; Martin, S. T.; Choi, W.; Bahnemann, D. W. Environmental Applications of Semiconductor Photocatalysis. *Chem. Rev.* **1995**, *95*, 69−96.
(38) Peller, J.; Wiest, O.; Kamat, P. V. Hydroxyl Radical's Role in the Remediation of a Common Herbicide, 2,4-Dichlorophenoxyacetic

https://doi.org/10.1021/acsphyschemau.1c00035
ACS Phys. Chem Au 2022, 2, 89−97

acid (2,4-D) -Feature Article. *J. Phys. Chem. A* **2004**, *108*, 10925−10933.
(39) Dieckmann, M. S.; Gray, K. A.; Kamat, P. V. Photocatalyzed Degradation of Adsorbed nitrophenolic Compounds on Semiconductor Surfaces. *Water Sci. Technol.* **1992**, *25*, 277−279.
(40) Schmelling, D. C.; Gray, K. A.; Kamat, P. V. Role of Reduction in the Photocatalytic Degradation of Trinitrotoluene. *Environ. Sci. Technol.* **1996**, *30*, 2547−2555.
(41) Biggs, A. I. A Spectrophotometric Determination of The Dissociation Constants of P-Nitrophenol and Papaverine. *Trans. Faraday Soc.* **1954**, *50*, 800−802.
(42) Oginawati, K.; Susetyo, S. H.; Rahmawati, S. I.; Kurniawan, S. B.; Abdullah, S. R. S. Distribution of Organochlorine Pesticide Pollution in Water, Sediment, Mollusk, and Fish at Saguling Dam, West Java, Indonesia. *Toxicol. Res.* **2021**, DOI: 10.1007/s43188-021-00094-1.
(43) Wania, F.; Mackay, D. Tracking the Distribution of Persistent Organic Pollutants. *Environ. Sci. Technol.* **1996**, *30*, A390−396A.
(44) Wolff, M. S.; Toniolo, P. G.; Lee, E. W.; Rivera, M.; Dubin, N. Blood-Levels of Organochlorine Residues And Risk Of Breast-Cancer. *J. Natl. Cancer Inst.* **1993**, *85*, 648−652.
(45) Hites, R. A.; Foran, J. A.; Carpenter, D. O.; Hamilton, M. C.; Knuth, B. A.; Schwager, S. J. Global Assessment of Organic Contaminants in Farmed Salmon. *Science* **2004**, *303*, 226−229.
(46) Muir, D. C. G.; Norstrom, R. J.; Simon, M. Organochlorine Contaminants in Arctic Marine Food-Chains - Accumulation of Specific Polychlorinated-Biphenyls and Chlordane-Related Compounds. *Environ. Sci. Technol.* **1988**, *22*, 1071−1079.
(47) Serpone, N.; Al-Ekabi, H.; Patterson, B.; Pelizzetti, B.; Minero, C.; Pramauro, E.; Fox, M. A.; Draper, R. B. Kinetic Studies in Heterogeneous Photocatalysis. II. The TiO_2 Mediated Degradation of 4-Chlorophenol Alone and In Three Component Mixture of Chlorophenol, 2,4-Dichlorophenol, and 2,4,5-Trichlorophenol. *Langmuir* **1989**, *5*, 250.
(48) D'Oliveira, J. C.; Al, S. G.; Pichat, P. Photodegradation of 2- and 3-Chlorophenol in TiO_2 Aqueous Suspensions. *Environ. Sci. Technol.* **1990**, *24*, 990−996.
(49) Stafford, U.; Gray, K. A.; Kamat, P. V. Radiolytic and TiO_2 Assisted Photocatalytic Degradation of 4-Chlorophenol. A Comparative Study. *J. Phys. Chem.* **1994**, *98*, 6343−6351.
(50) Vinodgopal, K.; Stafford, U.; Gray, K. A.; Kamat, P. V. Electrochemically Assisted Photocatalysis. II. The Role of Oxygen and Reaction Intermediates in the Degradation of 4-Chlorophenol on Immobilized TiO_2 Particles. *J. Phys. Chem.* **1994**, *98*, 6797−6803.
(51) Peller, J.; Wiest, O.; Kamat, P. V. Mechanism of Hydroxyl Radical-Induced Breakdown of the Herbicide 2,4-Dichlorophenoxyacetic Acid. *Chem. − Eur. J.* **2003**, *9*, 5379−5387.

https://doi.org/10.1021/acsphyschemau.1c00035
ACS Phys. Chem Au 2022, 2, 89−97